

Method for the simultaneous determination of vertical and horizontal mobilities in superlattices

C. H. Swartz* and T. H. Myers

Texas State University, Materials Science, Engineering and Commercialization Program, 601 University Drive, San Marcos, Texas 78666, USA

(Received 4 November 2013; published 10 February 2014)

A magnetoresistance method is proposed which extracts both the growth direction mobility and the planar mobility of an anisotropic thin film, such as a superlattice. A magnetic field which varies in magnitude and orientation is employed. Errors appearing in previous magnetotransport studies on superlattices are resolved. In particular, it is shown that the contact layers used to send currents through an active region do not have a negligible resistance, even if they are much more conductive than the active region. The technique is demonstrated on an InAs/GaSb-based structure where the growth axis to planar mobility anisotropy ratio is found to drop rapidly with increasing temperature.

DOI: [10.1103/PhysRevB.89.075305](https://doi.org/10.1103/PhysRevB.89.075305)

PACS number(s): 73.61.Ey, 73.50.Jt, 81.05.Ea

I. INTRODUCTION

The development of the III-V strained layer superlattice (SLS) is motivated by the ability to both tune the band gap and suppress the Auger recombination through proper tailoring of the layer thicknesses. For many IR applications, the system may prove superior to HgCdTe-based materials, which are hampered by large generation-recombination leakage currents and a need for delicate composition control to achieve band-gap tunability [1].

The SLS system has not yet lived up to its potential as carrier mobilities and lifetimes continue to be limited by extrinsic factors. Mobility is limited by roughness, and lifetime is limited by Shockley-Read-Hall recombination. An understanding of mobility, particularly along the vertical or growth direction, is crucial for device modeling and optimization [2]. In addition, the results of lifetime measurements may, in turn, depend upon the values assumed for vertical mobilities [3,4].

Whereas in-plane, or horizontal, mobilities are routinely measured [5], the direct measurement of vertical mobility has proven to be technically challenging. Theoretical calculations [6,7] have predicted both mobilities in terms of the dominant scattering mechanism, which is interface roughness. Such calculations have the drawback of a double-valued roughness correlation parameter for a given horizontal mobility so that knowledge of the horizontal mobility would provide, at best, two possible vertical mobilities.

To obtain experimental vertical mobility values, cyclotron resonance has been used to estimate scattering rates, yet the scattering rates measured in this way do not include angular dependence [8]. The potentially higher probability of backwards 180° scattering for vertically flowing charges should be a major factor in the mobility anisotropy [6], so one would expect such measurements to underestimate the anisotropy ratio. Time-of-flight measurements are another possible avenue; minority carriers created by an ultrafast laser pulse can diffuse vertically through a superlattice to a lower band gap well where a time-resolved change in photoluminescence is detectable. Such sophisticated measurements

might, however, be especially difficult to achieve at higher temperatures or on long-wavelength (LWIR) material [9].

Clearly, a magnetotransport solution would be desirable. To this end, geometric magnetoresistance (GMR) has been carried out on superlattices numerous times. By fabricating a pair of heavily doped contact layers on each face of a wide thin lightly doped active region (AR), the measured contact-to-contact resistance should be dominated by that AR. As a voltage is applied vertically between the two contact layers and a magnetic field is applied horizontally, the more conducting contact layers serve to short out the horizontal electric field in the AR. That is, the symmetry of the sandwich structure in Fig. 1 compels the Hall-effect voltage to become zero in the AR. This should result in a measured resistance R_0 increasing as $R_0[1 + (\mu B)^2]$ when a magnetic flux density B is applied horizontally ($\theta = 90^\circ$) on an AR with a given mobility μ [10].

GMR has been used for p - n junctions in HgCdTe where the saturation current was measured under the assumption that one of the two carrier types had a lower mobility and, thus, a negligibly small magnetoresistance [11,12]. Later, similar measurements were carried out on SLS structures by several groups, not only on p - n junctions [13], but also on p^+ - p^- - p^+ junctions [14,15], in order to confine the measurement to one carrier type. The latter was analyzed using quantitative mobility spectrum analysis (QMSA), which appeared to suggest a multitude of conducting pathways and carrier types.

However, all such attempts to probe vertical transport in SLSs by GMR have suffered from serious errors.

First, the mobility factor $[1 + (\mu B)^2]$ is only correct for isotropic materials. For an anisotropic SLS, the ratio between current density and electric field is found from the anisotropic conductivity tensor. As the electric field is limited to the vertical or x component and as the measured current density is likewise limited to the vertical, the relevant conductivity component is [16]

$$\sigma_{xx} = \sigma_0 \frac{1 + (\mu_{\parallel} B_{\perp})^2}{1 + (\mu_{\parallel} B_{\perp})^2 + \mu_{\parallel} \mu_{\perp} B_{\parallel}^2}, \quad (1)$$

where σ_0 is the zero-field conductivity in the vertical direction at $B = 0$ and the \perp and \parallel subscripts refer to the vertical (growth axis or x) and horizontal directions, respectively. Thus, for a

*Corresponding author. craig.swartz@txstate.edu

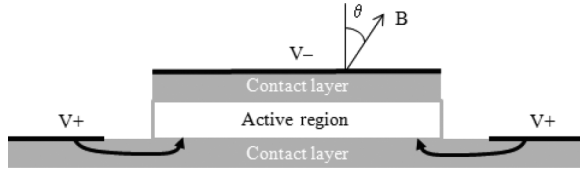


FIG. 1. A sandwich structure for GMR. Heavily doped contact layers surround an AR, such as a low doped SLS.

horizontally applied magnetic field, the original $\mu^2 B^2$ term becomes $\mu_{\parallel} \mu_{\perp} B_{\parallel}^2$, and the μ resulting from the standard GMR analysis would not be the vertical mobility but the geometric average of the horizontal and vertical mobilities μ_{\parallel} and μ_{\perp} .

Second, the series resistance of the contact layers is generally neglected. Although these highly doped layers have a much greater conductivity than the AR, the bottom contact layer resistance cannot be neglected unless its sheet resistivity is less than the resistance of the entire AR in ohms. Equivalently, the transfer length L_T traveled by the current before entering the AR must be considerably greater than the diameter of the structure under test. If R_S is the sheet resistivity of the contact layer, then $L_T^2 = \rho_c / R_S$ [17,18]. The “specific contact resistivity” in this instance takes the form $\rho_c = t / \sigma_{xx}$, which is the resistance-area product for a current density crossing an AR having a volume conductivity component σ_{xx} and a thickness t .

A typical SLS mesa used in a GMR measurement might have a contact layer with 100 times the dopant density of the AR but one quarter of its thickness. The sheet resistivity becomes $R_S = 4 / (100t\sigma_{xx})$, and the transfer length is then $L_T = 5t$. As mesa radii are generally several orders of magnitude greater than the thickness, L_T is much too short for the series resistance to be ignored. Any decrease in mobility in the contact layer with increased doping only compounds the effect. Moreover, this series resistance cannot be an additive term independent of B : Any magnetoresistance-related change in ρ_c changes the expected length L_T traveled by the current before entering the AR. Finally, placing the contact metallization closer to the base of the mesa cannot adequately reduce the effect.

This paper presents a method for a single magnetotransport determination of the separate horizontal and vertical mobilities in a superlattice or in any anisotropic thin film. It takes into account the series resistance effects, eliminating the need for a highly conducting substrate. Previous vertical conduction reports, which were difficult to interpret, are explained as well as some reports related to the Shubnikov–de Haas (SDH) effect. The method is demonstrated on an InAs/GaSb-based LWIR SLS doped in the $n^+ - n^- - n^+$ pattern.

II. THEORY

For a circular mesa of radius r surrounded by a large area ohmic contact on a film of sheet resistance R_S , the total resistance is

$$R_{\text{TOT}} = \frac{R_S}{2\pi} \left[\frac{L_T}{r} \frac{I_0(r/L_T)}{I_1(r/L_T)} + \frac{K_0(r/L_T)}{K_1(r/L_T)} \frac{L_T}{r+d} + \ln \left(1 + \frac{d}{r} \right) \right], \quad (2)$$

where d is the gap between the mesa and a large area metallization, which forms the connection to the contact layer, and I and K are the modified Bessel functions of the first and second kinds [17]. Fortunately, the Bessel function ratios simplify to one for $r \gg L_T$. In addition, a large area metallization can be replaced by a ring contact of known dimensions with the use of a somewhat lengthier formula [18].

When a magnetic field is oriented horizontally, the product of the vertical and horizontal mobilities ($\mu_{\parallel} \mu_{\perp}$) in an AR can be found from fitting the field dependence of R_{TOT} in Eq. (2) while using Eq. (1) to replace the transfer length with

$$L_T^2 = \frac{\rho_c}{R_S} = \frac{t}{R_S \sigma_{xx}} = \frac{t(1 + \mu_{\parallel} \mu_{\perp} B_{\parallel}^2)}{R_S \sigma_0}. \quad (3)$$

If μ_{\parallel} is already known, μ_{\perp} can be readily determined. If μ_{\parallel} is not already known, a tilted field technique is possible, not unlike earlier measurements used to distinguish contact resistance from bulk material spreading resistance in GaAs [19,20]. With B no longer limited to the horizontal, Eq. (1) gives the transfer length,

$$L_T^2 = \frac{t[1 + (\mu_{\parallel} B_{\perp})^2 + \mu_{\parallel} \mu_{\perp} B_{\parallel}^2]}{R_S \sigma_0 [1 + (\mu_{\parallel} B_{\perp})^2]}. \quad (4)$$

The sheet resistivity R_S of the contact layer is complicated by its own dependence on B . Since the contact layer is cylindrically symmetric, it forms what is known as a Corbino disk geometry. The symmetry prevents an angular electric field, compelling the Hall voltage to be zero just as it was in the sandwich structure. The sheet resistance of a Corbino disk is [10]

$$R_S = \frac{1 + (\mu_S B_{\perp})^2}{\sigma_{S0}}, \quad (5)$$

where μ_S is the contact layer mobility and σ_{S0} is the contact layer sheet conductivity at $B = 0$.

For a magnetic flux density of magnitude B tilted θ degrees from the vertical, Eqs. (5) and (4), respectively, become

$$R_S = \frac{1 + (\mu_S B \cos \theta)^2}{\sigma_{S0}} \equiv \frac{1}{\sigma_S(B, \theta)}, \quad (6)$$

and

$$L_T^2 = t \frac{1 + (\mu_{\parallel} B \cos \theta)^2 + \mu_{\parallel} \mu_{\perp} B^2 \sin^2 \theta}{R_S \sigma_0 [1 + (\mu_{\parallel} B \cos \theta)^2]} \equiv t \frac{\sigma_S(B, \theta)}{\sigma(B, \theta)}. \quad (7)$$

These are substituted into Eq. (2), which is fit to the measured total resistance using the two independent variables θ and B with the five parameters, σ_{S0} , μ_S , σ_0 , μ_{\parallel} , and $(\mu_{\parallel} \mu_{\perp})$. Note that σ_{S0} and σ_0 are the contact layer’s *sheet* conductivity and the AR’s *volume* conductivity, respectively.

In the case of multiple parallel conducting mechanisms in the AR, $\sigma(B, \theta)$ is additive so that [21]

$$\sigma(B, \theta) \rightarrow \sum_i \sigma_i(B, \theta). \quad (8)$$

Each conductivity $\sigma_i(B, \theta)$ introduces its own triplet of σ_0 , μ_{\parallel} , and $(\mu_{\parallel} \mu_{\perp})$ parameters. Similarly, $\sigma_S(B, \theta)$ would be additive for cases of multiple conducting contact layers.

Finally, in the case of contact through a highly conducting substrate, there is no series resistance from the contact layer, and R_{TOT} becomes simply

$$R_{\text{TOT}} = \frac{t}{\pi r^2 \sigma(B, \theta)}. \quad (9)$$

Only a three-parameter fit of σ_0 , μ_{\parallel} , and $(\mu_{\parallel}\mu_{\perp})$ would then be necessary.

III. EFFECTS ON MAGNETOTRANSPORT MEASUREMENTS

If a single conducting mechanism with a single mobility is present, the magnetoresistance term of ρ_c has a classic B^2 dependence. Thus, the total magnetoresistance in Eq. (2) would be approximately linear with B , a fact which has been previously interpreted by the QMSA algorithm as several closely competing parallel conducting mechanisms in SLSs [14].

Also, if the mesa radius r becomes smaller while remaining greater than L_T , the total resistance increases as $\sim 1/r$ rather than $\sim 1/r^2$. This means that the measured current increases linearly with the radius, a fact that had previously been attributed to heavy dominant sidewall conduction when analyzing mesas of various sizes [15].

Photocurrent measurements in a SLS have found an induced minigap shift under an applied magnetic field, a shift which appeared to be halved when the field was applied in the growth direction [22]. This is likely due to the contact layer having a different minigap and its magnetoresistance beginning to dominate the current when the field takes the vertical orientation.

Similar effects occur on AlGaAs/GaAs superlattices during SDH measurements where electrons flowing through the AR appear to have their properties somehow modulated by the contact layer [23]. In fact, when the B orientation is vertical, the magnetoresistance of the contact layer itself is being measured, not that of the AR.

Studies undertaken with a fully conducting substrate would not be affected by the series resistance, provided that the substrate's conductivity σ_{sub} is high enough for the measured resistance to be much greater than the spreading resistance R_{sp} , which is roughly [17]

$$R_{\text{sp}} = \frac{1}{4r\sigma_{\text{sub}}}. \quad (10)$$

Whereas, AlGaAs/GaAs superlattices are often grown on fairly conducting substrates ($n \sim 10^{18} \text{ cm}^{-3}$ GaAs), the σ_{sub} remains below the $1000 (\Omega \text{ cm})^{-1}$ range [24]. Given a mesa 50–100 μm across, a R_{sp} of one quarter of an ohm may not only be present, but also can increase at higher magnetic fields due to the Corbino effect [25]. This becomes significant when the measured resistance is only a few ohms. Several studies have attempted to measure magnetophonon resonance in these superlattices using a vertical field [26,27], but the field dependence of the GaAs spreading resistance beneath the superlattice would interfere with determining the derivatives of conductivity with B . A similar issue affected at least one SLS study; although the AR resistance was higher in that case, the InAs substrate had a lower doping level with a higher mobility

[28]. This would have yielded a higher magnetoresistance for R_{sp} . Although the experimental results from these conducting substrate studies may be qualitatively valid, the peak positions are in need of reassessment.

IV. EXPERIMENTAL DETAILS

Superlattices were grown by molecular-beam epitaxy on a GaSb substrate with a 100-nm homoepitaxial smoothing layer. A 500-nm bottom contact layer of $n\text{-InAs}_{0.91}\text{Sb}_{0.09}$ ($\text{Si} \sim 10^{18} \text{ cm}^{-3}$) provided a shorting effect to reduce the complexity associated with currents passing through the substrate. This was followed by a superlattice consisting of 660 periods of 2.1 nm of GaSb and 4.4 nm of InAs. The first and final 16 periods were each doped with $6 \times 10^{10} \text{ cm}^{-2}$ of Si in the InAs layer, and the 618 periods between were left unintentionally doped to form an $n^+n^-n^+$ structure. Finally, a 10-nm thickness of $n\text{-InAs}$ ($\text{Si} \sim 10^{18} \text{ cm}^{-3}$) served as a cap layer.

Circular unpassivated mesas of radius $r = 350 \mu\text{m}$ were formed by etching in a citric acid/hydrochloric acid/peroxide mixture to a depth of 3.9 μm so that nearly all of the undoped region was confined to the mesas. Beyond a gap of $d = 150 \mu\text{m}$, the area outside of the mesas was covered in a wide area ohmic contact metallization. The opposite metal contact covered the top of the mesa. Both metallizations were made of sputtered Ti/Au-Pd.

Angle- and field-dependent resistance measurements were carried out in a Quantum Design physical property measurement system at 22 values of B from 0 to 9 T and in 2° steps at each field value. The temperature was varied from 20 to 300 K. The data were fit to Eq. (2) with the substitution of (6) and (7) using the standard Levenberg-Marquardt algorithm.

As the dataset and parameter space can become quite large, it was necessary to, at first, confine the fit to the data at $\theta = 0^\circ$ and 90° from normal, leaving out the μ_{\parallel} parameter while obtaining the other four. During this stage, parallel conducting layers can be introduced using Eq. (8) if necessary to explain the B -dependent data. Afterwards, the full set of angle-dependent data were fit to find all five parameters, including μ_{\parallel} using the recently obtained four parameters as guess values.

V. RESULTS AND DISCUSSION

The field dependence at 90° is dominated by the sandwich structure GMR of the AR, and the field dependence at 0° is dominated by the Corbino GMR of the contact layer. A fit to the 90° data in Fig. 2 was significantly improved by a parallel conducting layer. Although previous reports concluded the existence of sidewall leakage based on a potentially flawed variable area analysis, the sidewall, which is unpassivated in our case, does remain the most reasonable assignment for the source of a parallel conducting path. The contribution of the sidewall is somewhat small as the same values for mobilities and conductivities could still be obtained within $\sim 30\%$ even when eliminating the sidewall from the analysis.

The fit to the 0° field-dependent data could not be appreciably improved by any parallel conducting layers. This implies that only one significant conducting path with a single

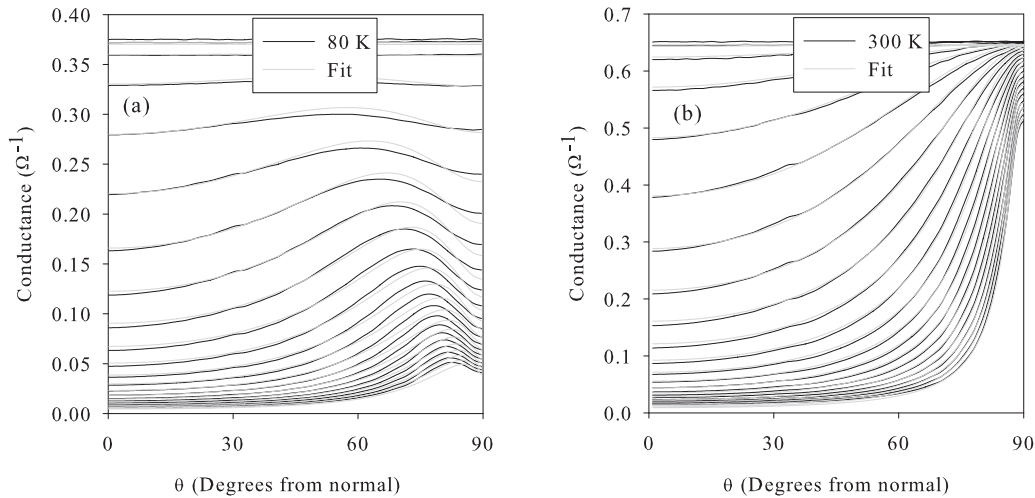


FIG. 2. Typical field-angle-dependent conductance at (a) 80 K and (b) 300 K. The contact layer dominates near 0°, whereas, the 90° results from the AR. The highest line represents a magnetic field of $B = 0.05$ T, and the lowest line represents $B = 9$ T.

mobility was present in the contact layer, presumably the $\text{InAs}_{0.91}\text{Sb}_{0.09}$ layer. Note that, although contact layers can be made entirely from heavily doped versions of the same superlattice structure as the AR, the mobility values found in the two regions would not be similar due to a very strong dependence of horizontal mobility on carrier concentration, which has been both predicted and observed [5,6].

The resultant mobilities and conductivities are shown in Figs. 3 and 4. To confirm the soundness of the fitting analysis, a Van der Pauw measurement of the $\text{InAs}_x\text{Sb}_{1-x}$ contact layer alone was performed by etching $3.9 \mu\text{m}$ of the film, confining the remainder to a cloverleaf geometry. The field dependence of the sheet resistivity was, indeed, found to match Eq. (5) with a mobility μ_S of $18\,000\text{--}20\,000 \text{ cm}^2 \text{ V}^{-1} \text{ s}^{-1}$ in agreement with the Corbino disk mobility value shown in Fig. 3.

The conductivity of the AR (the undoped SLS layer) is displayed as carrier concentration. The parameters had a

standard error of less than 10% when under 200 K. Over 200 K, they quickly became less reliable due to a smaller share of total measured resistance originating in the AR as can be seen in the 90° data of Fig. 2(b). At temperatures below 20 K, SDH oscillations became visible in the data and prevented the fitting analysis from being carried out. It is possible that the displacement appearing in the 20-K mobilities and concentrations is due to a distortion of the fit from this effect.

The SLS horizontal mobility is about $40\,000 \text{ cm}^2 \text{ V}^{-1} \text{ s}^{-1}$ and remains high as the vertical mobility drops. From this analysis, it appears that vertical mobility is dramatically lower than the horizontal in this superlattice, but such differences in mobility are not unexpected theoretically (compare with Figs. 2 and 3 of Ref. [7]). As roughness correlation lengths become greater than 30 nm, the horizontal mobility is predicted to increase quickly, whereas, the vertical mobility more or less saturates. The same effect is compounded by higher electron concentrations and is compounded further by raising the

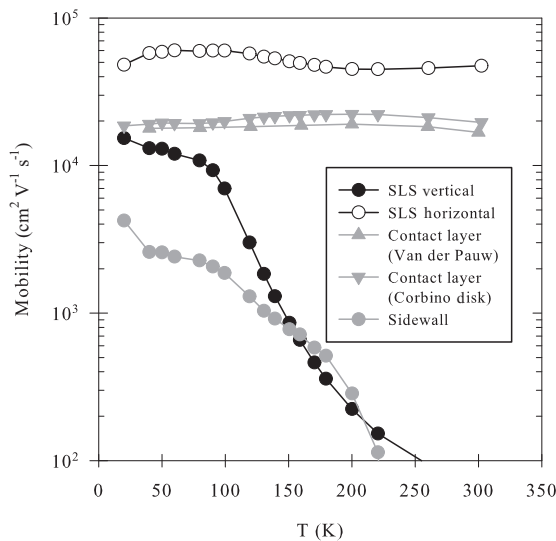


FIG. 3. Temperature dependence of the fitted carrier mobility for the SLS, the contact layer, and the additional parallel conducting layer potentially caused by sidewall conduction.

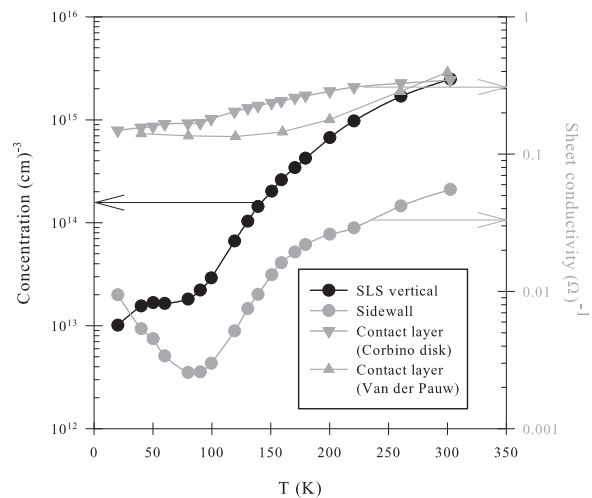


FIG. 4. Temperature dependence of the fitted carrier concentration as well as the sheet conductivities of the contact layer and the parallel conducting layer potentially caused by sidewall conduction.

temperature above 0 K, independently of increases in carrier concentration [6,7]. Interestingly, the horizontal mobility shows no signs of any scattering mechanism aside from roughness, such as the optical phonon scattering commonly seen near room temperature in bulk compound semiconductors.

VI. CONCLUSIONS

A method of extracting horizontal and vertical mobilities from a single measurement on an anisotropic film is proposed. The method also extracts the properties of the contact layer. This layer's inclusion in the analysis explains erroneous results appearing in all previous attempts to probe III-V SLS vertical

mobilities by magnetotransport as well as several other studies involving SDH oscillations. The method was demonstrated on a GaSb-InAs superlattice where it was found that vertical mobility is much smaller than horizontal mobility and that the anisotropy ratio increases with temperature.

ACKNOWLEDGMENTS

We would like to thank K. Clark of IntelliEPI for the growth of the structure. This work was supported by the DARPA SBIR program under Contract No. W911NF-09-C-0120 subcontracted through Amethyst Research, Inc.

-
- [1] C. H. Grein, J. Garland, and M. E. Flatte, *J. Electron. Mater.* **38**, 1800 (2009).
- [2] I. Vurgaftman, C. L. Canedy, E. M. Jackson, J. A. Nolde, C. A. Affouda, E. H. Aifer, J. R. Meyer, A. Hood, A. J. Evans, and W. T. Tennant, *Opt. Eng.* **50**, 061007 (2011).
- [3] L. Zheng, M. Tidrow, S. Bandara, L. Aitchison, and T. Shih, *Proc. SPIE* **8012**, 80120S (2011).
- [4] B.-M. Nguyen, G. Chen, M.-A. Hoang, and M. Razeghi, *Proc. SPIE* **7945**, 79451O (2011).
- [5] F. Szmulowicz, S. Elhamri, H. J. Haugan, G. J. Brown, and W. C. Mitchel, *J. Appl. Phys.* **105**, 074303 (2009).
- [6] F. Szmulowicz, H. J. Haugan, S. Elhamri, and G. J. Brown, *Phys. Rev. B* **84**, 155307 (2011).
- [7] F. Szmulowicz, H. J. Haugan, S. Elhamri, and G. J. Brown, *Infrared Phys. Technol.* **56**, 76 (2013).
- [8] S. Suchalkin, G. Belenky, S. P. Svensson, B. Laikhtman, D. Smirnov, L. C. Tung, and S. Bandara, *J. Appl. Phys.* **110**, 043720 (2011).
- [9] B. V. Olson, L. M. Murray, J. P. Prineas, M. E. Flatte, and J. T. Olesberg, *Appl. Phys. Lett.* **102**, 202101 (2013).
- [10] P. Blood and J. W. Orton, *The Electrical Characterization of Semiconductors: Majority Carriers and Electron States* (Academic, Waltham, MA, 1992).
- [11] S. E. Schacham and E. Finkman, *J. Vac. Sci. Technol. A* **7**, 387 (1989).
- [12] N. T. Gordon, S. Barton, P. Capper, C. L. Jones, and N. Metcalfe, *Semicond. Sci. Technol.* **8**, S221 (1993).
- [13] L. Bürkle, F. Fuchs, R. Kiefer, W. Pletschen, R. E. Sah, and J. Schmitz, *Electrical Characterization of InAs/(GaIn)Sb Infrared Superlattice Photodiodes for the 8 to 12 μ m Range*, MRS Symposia Proceedings No. 607 (Materials Research Society, Pittsburgh, 2000), p. 77.
- [14] G. A. Umana-Membreno, B. Klein, H. Kala, J. Antoszewski, G. Gautam, M. N. Kutty, E. Plis, J. M. Dell, S. Krishna, and L. Faraone, *Proc. SPIE* **8012**, 80120Y (2011).
- [15] G. A. Umana-Membreno, B. Klein, H. Kala, J. Antoszewski, N. Gautam, M. N. Kutty, E. Plis, S. Krishna, and L. Faraone, *Appl. Phys. Lett.* **101**, 253515 (2012).
- [16] H. J. Mackey and J. R. Sybert, *Phys. Rev.* **180**, 678 (1969).
- [17] D. K. Schroder, *Semiconductor Material and Device Characterization* (Wiley, Hoboken, NJ, 2006).
- [18] G. K. Reeves, *Solid-State Electron.* **23**, 487 (1980).
- [19] L. Gútai and I. Mojzes, *Appl. Phys. Lett.* **26**, 325 (1975).
- [20] A. Woldenberg, T. Prezlowski, and J. Klamka, *Solid-State Electron.* **35**, 61 (1992).
- [21] J. S. Kim, D. G. Seiler, and W. F. Tsing, *J. Appl. Phys.* **73**, 8324 (1993).
- [22] F. Fuchs, E. Ahlswede, U. Weimar, W. Pletschen, J. Schmitz, M. Hartung, B. Jager, and F. Szmulowicz, *Appl. Phys. Lett.* **73**, 3760 (1998).
- [23] F. Aristone, J.-C. Portal, J. F. Palmier, and J. C. Harmand, *Braz. J. Phys.* **29**, 375 (1999).
- [24] R. O. Grendin, *Appl. Phys. Lett.* **54**, 2438 (1989).
- [25] D. Schuocker, *Electron. Lett.* **6**, 275 (1970).
- [26] P. Gassot, J. Genoe, D. K. Maude, J. C. Portal, K. S. H. Dalton, D. M. Symons, R. J. Nicholas, F. Aristone, J. F. Palmier, and F. Laruelle, *Phys. Rev. B* **54**, 14540 (1996).
- [27] H. Noguchi, H. Sakaki, T. Takamasu, and N. Miura, *Phys. Rev. B* **45**, 12148 (1992).
- [28] R. S. Deacon, R. J. Nicholas, P. A. Shields, and A. B. Henriques, *Phys. Rev. B* **76**, 075309 (2007).